Food Chemistry 405 (2023) 134892

Contents lists available at ScienceDirect

Food Chemistry

journal homepage: www.elsevier.com/locate/foodchem

PEF treatment effect on plant tissues of heterogeneous structure no longer an enigma: MRI insights beyond the naked eye

Jessica Genovese [a], Marko Stručić [b], Igor Serša [c], Vitalij Novickij [d,e], Pietro Rocculi [a], Damijan Miklavčič [b], Samo Mahnič-Kalamiza [b], Matej Kranjc [b,*]

[a] University of Bologna, Alma Mater Studiorum, Department of Agricultural and Food Sciences, P. Goidanich 60, Cesena, Italy
[b] University of Ljubljana, Faculty of Electrical Engineering, Tržaška c. 25, 1000 Ljubljana, Slovenia
[c] Jožef Stefan Institute, Jamova c. 39, 1000 Ljubljana, Slovenia
[d] Vilnius Gediminas Technical University, Faculty of Electronics, High Magnetic Field Institute, Naugarduko g. 41, 03227 Vilnius, Lithuania
[e] State Research Institute Centre for Innovative Medicine, Department of Immunology, Santariškių g. 5, Vilnius 08410, Lithuania

ARTICLE INFO

Keywords:
Pulsed electric fields
Magnetic resonance imaging
T2 relaxation time mapping
Electric field distribution
Plant tissue structure
Electroporation

ABSTRACT

Alteration of cell membrane permeability by exposure of plant tissues to pulsed electric fields (PEF) is associated with physical changes in cellular and subcellular structures. The aim of our study was to investigate the possible non-uniform effect of PEF treatment due to the structural heterogeneity of plant tissues commonly used in industrial PEF applications: apple fruits, potato tubers, and carrot taproots. Spatial distribution of T_2 relaxation times was measured using magnetic resonance imaging in relation to local electric field established during PEF treatment and measured by magnetic resonance electrical impedance tomography. The results showed an increasingly inhomogeneous distribution of T_2 relaxation times with increasing complexity of the structure (carrot > potato > apple). Feasibility and considerable potential for the use of the T_2 mapping technique in the analysis of the effects of PEF on plant tissue structures was demonstrated.

1. Introduction

Pulsed electric field (PEF) applications in food have focused on improving processes based on the ability of PEF technology to improve mass transfer, such as increasing the kinetics of drying (Tylewicz et al., 2022; Wiktor et al., 2016), increasing the yield of fruit juice extraction (Mahnič-Kalamiza et al., 2015; Praporscic et al., 2007), improving the release and bioaccessibility of valuable compounds (Canelli et al., 2022; Gagneten et al., 2019), and facilitating the reduction of toxicants (Genovese et al., 2019; Schouten et al., 2020) to list the most prominent and often studied applications. PEF treatment is based on the process of electroporation, a phenomenon that leads to an increase of cell membranes permeability in a tissue exposed to high-voltage electric pulses. Electroporation is considered a threshold phenomenon, and is therefore dependent on local electric fields (Kotnik et al., 2012; Mahnič-Kalamiza, Vorobiev, et al., 2014; Mahnič-Kalamiza & Miklavčič, 2022). It is most often explained by the formation of hydrophilic pores in the lipid domain of the cell membrane (Kotnik et al., 2019), which increases the conductance of the membrane and the permeability of this hydrophobic barrier to mass transfer.

As previously demonstrated, the change of the cell membrane permeability due to the exposure of biological tissues to PEF – especially of plant tissues – is also associated with physical changes in cellular and subcellular structures, i.e. changes in intra-cellular and extra-cellular volumes, as well as in the volume of the vacuole (Dellarosa et al., 2018; Menegazzo et al., 2020), and consequently with the leakage of water and dissolved solutes from the intra- to the extra-cellular space (Mahnič-Kalamiza, Miklavčič, et al., 2014). Understanding such changes in the target food materials is of great importance for the desired treatment outcome.

Magnetic resonance imaging (MRI) techniques have been used to monitor the spatially-dependent effect of PEF treatment in plant tissues (Dellarosa et al., 2018; Kranjc et al., 2016). Proton (^{1}H) NMR imaging (MRI) and relaxation time mapping are very powerful tools for the study of plant-based foods, as they are sensitive to the mobility of water in the microscopic environment of the tissue. ^{1}H NMR signal is proportional to the water distribution in the tissue, and can therefore provide valuable information about the anatomical details of the tissue (Kamal et al., 2019; Patel et al., 2015). NMR relaxation time mapping can provide additional information on the microstructure of plant tissues and of the

* Corresponding author.
E-mail address: matej.kranjc@fe.uni-lj.si (M. Kranjc).

https://doi.org/10.1016/j.foodchem.2022.134892
Received 13 June 2022; Received in revised form 4 November 2022; Accepted 5 November 2022
Available online 11 November 2022

water microenvironment (Collewet et al., 2022; Hills, 1995; Hills & Duce, 1990). Specifically, the transverse relaxation time T_2 (also known as spin–spin relaxation time) has been used as an indication of the redistribution of water and solutes in the tissue after the PEF treatment (Genovese et al., 2021; Hjouj & Rubinsky, 2010). In addition, magnetic resonance electrical impedance tomography (MREIT) has been proposed as a method for monitoring the electric field distribution in the tissue during PEF treatment (Kranjc et al., 2011). MREIT is based on current density imaging (CDI), an MRI technique for measuring current density distribution, followed by reconstruction of the electric field distribution using numerical algorithms. MREIT has made rapid progress over the last decade, particularly in imaging the electrical conductivity of biological tissue (Seo & Woo, 2014). It is important to be aware that with the MREIT technique, the accumulative effect of electric current on the MRI signal phase is measured. Therefore, MREIT provides a time average of electric field distribution established during PEF treatment (Kranjc et al., 2012).

In our study, we selected three types of plant food tissues that have different structural complexity and are often used in industrial PEF applications, namely apple fruit (hereafter referred to as apple), potato tuber (hereafter referred to as potato) and carrot taproot (hereafter referred to as carrot). We have also chosen these plant tissues because they are of particular interest as model tissues for studies on medical applications of electroporation (Campana et al., 2016; Hjouj & Rubinsky, 2010). In our study, we aimed to investigate the possible non-uniform effect of PEF treatment due to the structural heterogeneity of plant tissues. We used MREIT to measure the spatial distribution of the electric field during PEF treatment, and T_2 mapping to measure change in T_2 relaxation times over the course of 6 h after treatment to investigate the relationship between the local electric field and tissue structures.

2. Material & methods

2.1. Plant tissues

The apples (*Malus domestica*, cv 'Golden Delicious'), potatoes (*Solanum tuberosum*, cv 'Liberta') and carrots (*Daucus carota*, cv 'Danvers') used for this study were purchased at the local market (Ljubljana, Slovenia). Before the experiments, structurally similar sections of each plant type were selected first and then manually cut with a sharp stainless-steel cork-borer into cylindrical samples of 26 mm in diameter and 30 mm in height. For each sample, the analyses were carried out in three replicates of different fruits/vegetables.

2.2. Experimental setup

2.2.1. PEF treatment

PEF treatment of the cylindrical-shape plant samples was performed using an electric pulse generator lab prototype (Novickij et al., 2016) connected to a pair of custom-built needle electrodes inserted into the sample tissue. The electrodes, made of platinum/iridium alloy (Pt/Ir: 90/10 %), had a diameter of 1 mm, and were placed at a fixed centre-to-centre distance of 10.4 mm. The PEF treatment protocol consisted of 2 sequences of 4 pulses with a duration of 100 μs and with a repetition frequency of 5 kHz. For potato and carrot tissues, the voltage of electric pulses was 750 V. Since apple tissue has a lower electrical conductivity compared to potato and carrot (Genovese et al., 2021), the voltage of electric pulses was increased to 1200 V in order obtain sufficient signal from phase images of Current Density Imaging (CDI) sequence (Serša et al., 1994). The trigger input of the generator was connected to the MRI spectrometer and synchronized with the CDI pulse sequence. The delivery of the electric pulses was monitored with an oscilloscope (WavePro 7300A, LeCroy, NY, USA) and a current probe (AP015, LeCroy, NY, USA).

2.2.2. T_2 mapping

Plant tissues were monitored by the T_2 mapping before PEF treatment and sequentially every hour until 6 h after PEF treatment. A multi-spin-echo (MSE) imaging sequence based on the Carr-Purcell-Meiboom-Gill (CPMG) multi-echo train (Carr & Purcell, 1954) was chosen to acquire a set of differently T_2-weighted MR images before and after applying the PEF treatment (i.e. 18 min after PEF treatment and every hour for the following 6 h). The MRI scanner consisted of a 2.35 T (100 MHz proton nuclear MR frequency) horizontal bore superconducting magnet (Oxford Instruments, Abingdon, UK) connected to an Apollo spectrometer (Tecmag, Houston TX, USA) and equipped with micro-imaging accessories with maximum gradients of 250 mT/m (Bruker, Ettlinger, Germany). Pulse sequence imaging parameters were the following: field of view 30 mm; imaging matrix 128 × 128; inter-echo delay 70 ms; number of echoes 8. Slice thickness was initially set at 5.1 mm but was later reduced to 3 mm as the signal-to-noise ratio (SNR) was high enough not to impact the quality of data. The calculation of T_2 maps was performed using the MRI Analysis Calculator plug-in of the ImageJ (NIH, Bethesda, MD, USA) image-processing software, fitting raw MSME (Multi-Slice-Multi-Echo) data at variable echo-time ($R^2 > 0.9$). Additional analysis and quantitative assessment of T_2 -weighted images was performed using MATLAB 2021b (MathWorks, Natick, MA, USA) on a desktop personal computer.

2.2.3. Magnetic resonance electrical impedance tomography

Magnetic resonance electrical impedance tomography (MREIT) was performed on plant tissues while applying the PEF treatment, following the method described in (Kranjc et al., 2016). The samples were scanned by the current density imaging (CDI) method during the application of the electric pulses in order to acquire a map of the current-induced magnetic field change in the sample. This can be detected via the phase shift registration by MRI (Joy, Scott, & Henkelman, 1989). The map was then processed using the magnetic resonance electrical impedance tomography (MREIT) J-substitution algorithm, based on iterative solving of the Laplace equation (Khang et al., 2002). The CDI data along with known sample geometry and potentials on the electrodes were used as inputs for the MREIT algorithm to calculate the conductivity map and the electric field distribution in the plant tissues. In this study, the two-shot rapid acquisition with relaxation enhancement (RARE) CDI pulse sequence (Figure S-1) was performed (Serša, 2008), and the following imaging parameters were used: field of view 30 mm; imaging matrix 64 × 64; inter-echo delay 2.64 ms. Slice thickness was initially set at 8 mm but was later reduced to 3 mm as the SNR was high enough not to impact the quality of data. In the sequence, the block of electroporation pulses was positioned between the excitation RF pulse and the first refocusing RF pulse. MREIT algorithm was solved using the finite element method with the numerical computational environment MATLAB 2021b (MathWorks, Natick, MA, USA) on a desktop personal computer.

2.2.4. Statistical analysis

Significant differences among the results were evaluated by parametric analysis of variance (ANOVA) and Tukey multiple comparison, with a significance level of 95 % ($p < 0.05$). When the Shapiro-Wilk test for normality and Levene's test for homoscedasticity of the data yielded statistically significant results ($p < 0.05$), the Kruskal-Wallis non-parametric multiple range test and Holm's stepwise adjustment with a significance level of 95 % ($p < 0.05$). Results are expressed as mean ± standard deviations of replications ($n = 3$). Statistical analysis was performed in R Statistical Software (R Foundation for Statistical Computing, Vienna, Austria).

3. Results and discussions

3.1. Spatial characterization of plant tissue structures, T_2 times and electric field

Fig. 1A shows T_2 – weighted images of each type of plant tissue: apple, potato, and carrot. On each of the images, detailed internal structure can be identified based on the variation of signal intensity. Based on the sampling procedure used in this experiment (i.e. sample cut perpendicularly to the longitudinal axis of the tissue), it is possible to distinguish only the outer cortex parenchyma of the apple fruit. In terms of water distribution, the apple parenchyma is the most homogeneous tissue along the plane of observation compared to the other two tissue types, i.e., of the potato tuber and carrot. In potato tuber, two parenchyma regions can be clearly distinguished, the inner and outer medulla. The inner medulla (also known as the pith) of the potato tuber forms what is known as the 'water-core' parenchyma. The inner medulla is a conductive tissue, lower in starch compared to the outer medulla (also referred to as perimedullary region). The perimedullary zone (internal phloem region), on the other hand, is the storage parenchyma, characterised by a high concentration of starch (Reeve, 1969). Finally, the carrot taproot presents the most complex structure compared to the apple and potato, in which the core of the central cylinder contains the parenchymatous xylem, in which vascular rays can be seen, and which is surrounded by the vascular cambium. The central cylinder is surrounded by a secondary phloem and cortex parenchyma. The xylem is a water-filled structure with lignified cell walls, mainly responsible for the transport of water and minerals, while the phloem consists mainly of densely packed, thin-walled cells and is responsible for the transport of nutrients (Esau, 1940).

The measured baseline, i.e. before the PEF treatment, spin–spin relaxation times (T_2) made it possible to identify these different structures of the tissues based on their water content. As can be seen in Fig. 1B, each of the previously described plants has an increasingly inhomogeneous distribution of T_2 relaxation times in the plane of observation with an increasing complexity of the structure (i.e. carrot > potato > apple). In addition to T_2 mapping, the electric field distribution using MREIT was determined during PEF (Fig. 1C). The non-uniformity of the obtained electric field distribution is primarily a consequence of the needle electrodes and the heterogeneity of the electrical conductivity due to the presence of different tissue structures.

3.2. Apple

Fig. 2 shows the measured dynamics of changes in T_2 relaxation times in the cortex of the apple exposed to the PEF treatment. Fig. 2A shows a T_2-weighted image scanned before PEF treatment where also three regions of interest of apple cortex are indicated (R1-3$_{cx}$). As can be observed, the electric field distribution in the cortex of the apple (Fig. 1C) is the highest in the region close to the electrodes, R1$_{cx}$ with

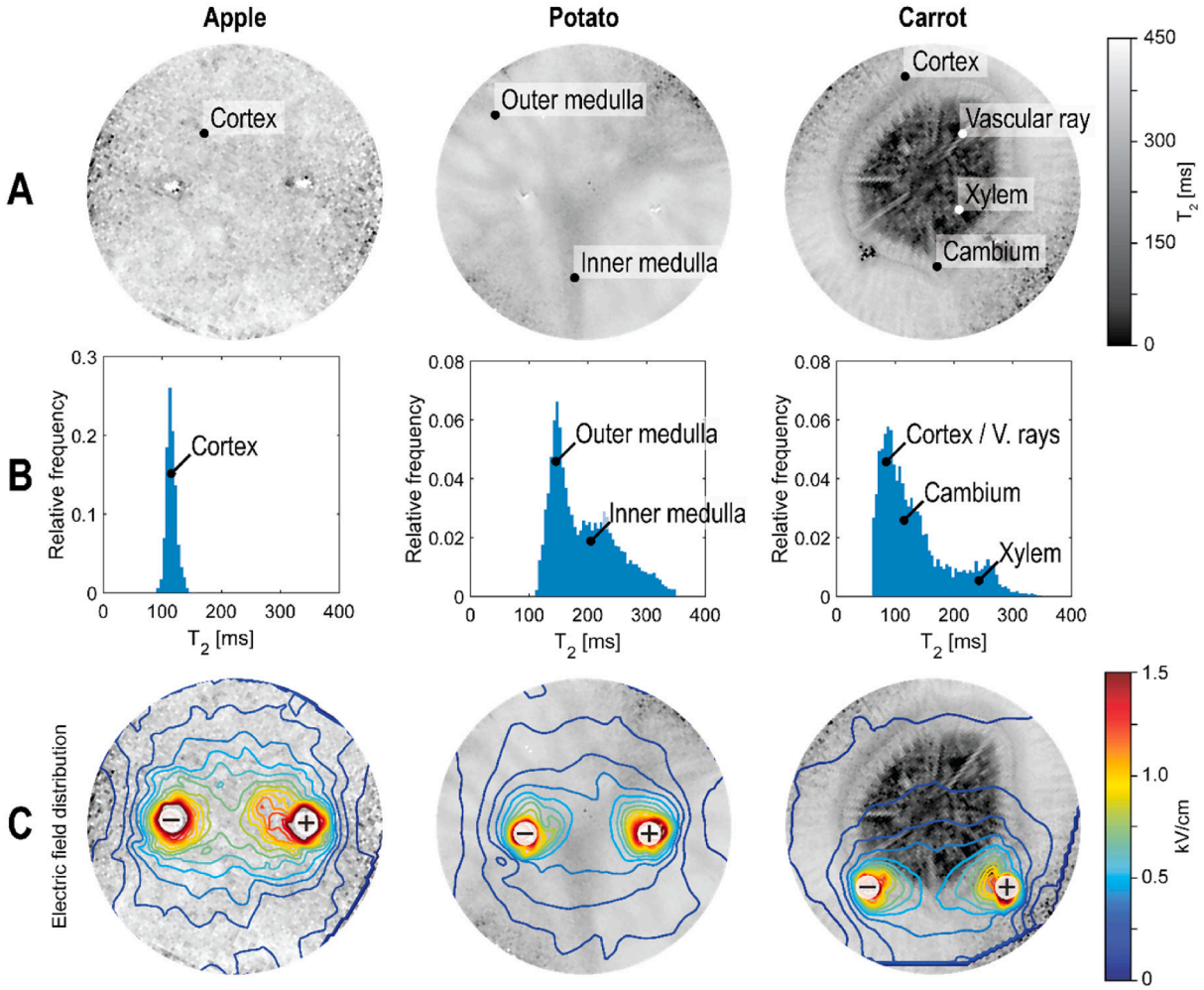

Fig. 1. Evaluation of T_2 relaxation time distributions and electric field distributions within the different tissue structures of plants. **A**: T_2 – weighted images of apple, potato and carrot with labelled tissue structures. **B**: Distribution of T_2 values within the different tissue structures before application of PEF treatment. **C**: Measured electric field distributions during PEF treatment.

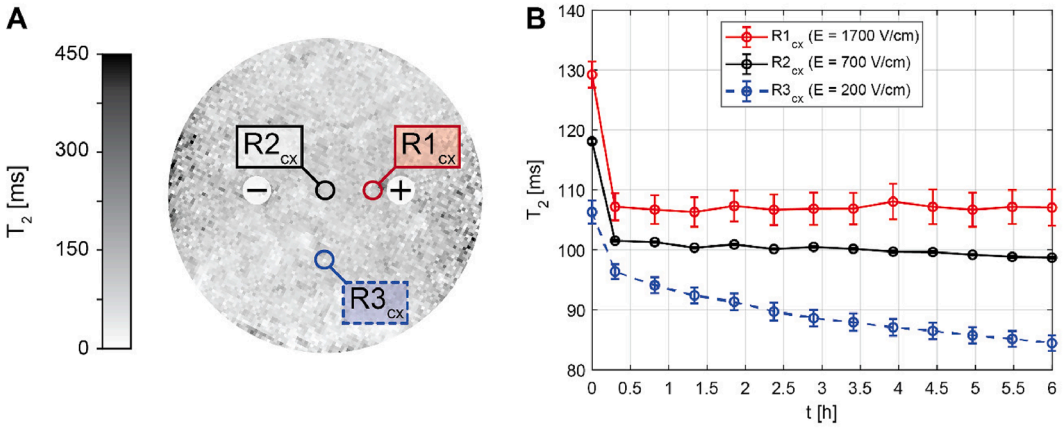

Fig. 2. Evaluation of T_2 values in the cortex of the apple exposed to PEF. **A**: T_2 values were evaluated in three Regions of interest (R1-3$_{cx}$), each exposed to different electric field. The locations of the electrodes are marked with + and -. **B**: Time course of T_2 values within R1-3$_{cx}$. Each time point represents a mean of T_2 ± standard deviation from the region of interest. Time point $t = 0$ shows T_2 values before the application of PEF.

1700 V/cm, while the electric field decreases with increasing distance from the electrodes, R2$_{cx}$ and R3$_{cx}$ reaching 700 V/cm and 200 V/cm, respectively. The T_2 values before and after the PEF treatment in R1-3$_{cx}$ are shown in Fig. 2B. In general, T_2 significantly decreases immediately after PEF treatment (i.e. 18 min after PEF), with R1$_{cx}$ showing the largest decrease in T_2, which decreases from 129 ± 0.002 to 107 ± 0.002 ms. Similar decrease in T_2 is observed in the region between the electrodes (R2$_{cx}$). In R3$_{cx}$, although the lowest electric field (200 V/cm) was measured, it is still high enough to cause a consistent and significant drop in T_2 values. However, in contrast to R1$_{cx}$ and R2$_{cx}$ the T_2 dynamics in R3$_{cx}$ is different as continuous decrease in T_2 times was measured throughout the observation period. The results of statistical analysis obtained with ANOVA are shown in Table S-1 (see Supplementary material).

Field strengths greater than 150 V/cm have been reported to alter subcellular compartmentalization of apple parenchyma when 20 pulses at 100 μs of duration were applied (Dellarosa et al., 2016). Despite the fact that in this study the tissue was exposed to the electric pulses for a

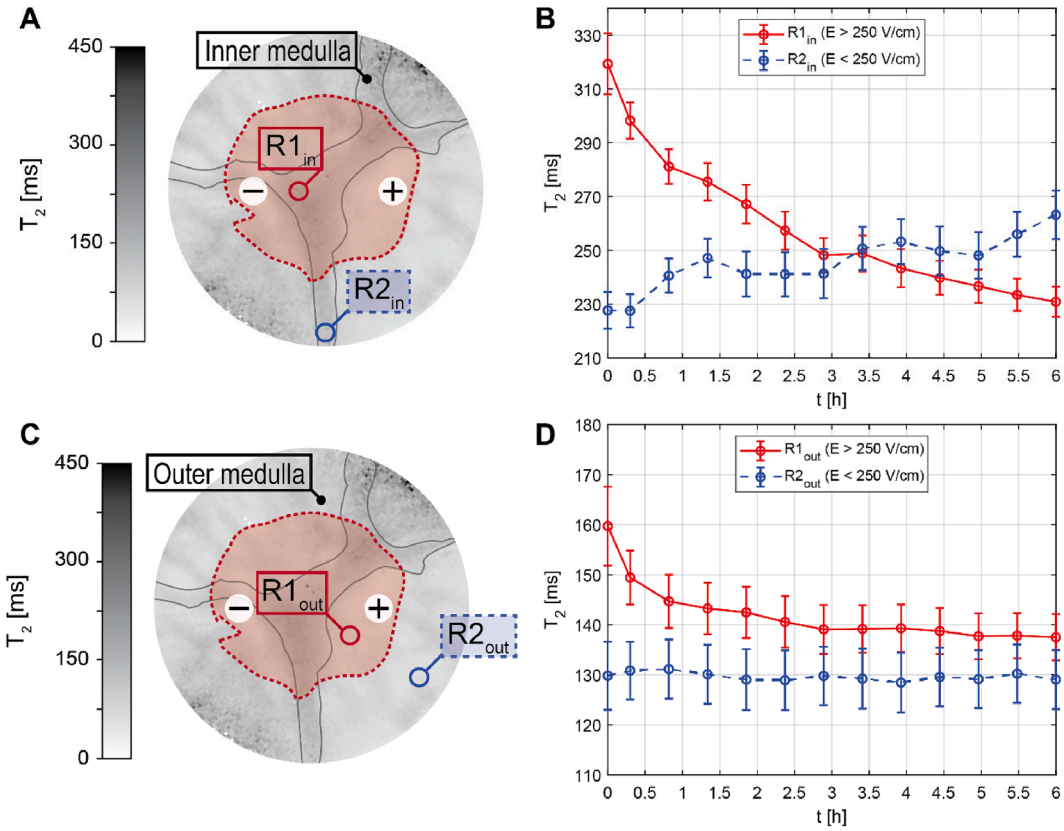

Fig. 3. Evaluation of T_2 values in the inner and outer medulla of the potato tuber exposed to PEF. **A, C**: An area of the potato that was exposed to an electric field greater than 250 V/cm is shaded in red. T_2 values were evaluated in two Regions of interest in the inner medulla (R1-2$_{in}$), and in the outer medulla (R1-2$_{out}$). R1$_{in,out}$ and R2$_{in,out}$ were in the region exposed to an electric field greater and less than 250 V/cm, respectively. The inner medulla is marked with a grey solid line for better visualization. The locations of the electrodes are marked with + and -. **B, D**: Time course of T_2 values within R1$_{in,out}$ and R2$_{in,out}$. Each time point represents a mean of T_2 ± standard deviation from the region of interest. Time point $t = 0$ shows T_2 values before the application of PEF. Note different ranges of T_2 in B and D.

shorter period of time (i.e. lower number of pulses applied), changes in T_2 values are comparable, suggesting that the electric field 200 V/cm (8 pulses at 100 μs of duration) was sufficient to trigger electroporation. Due to the low electrical conductivity of the apple, the electric pulse voltage had to be increased to obtain a sufficient signal from phase images of CDI sequence, as previously reported in (Genovese et al., 2021). Therefore, the entire volume of the apple sample was subjected to an electric field above the electroporation threshold.

3.3. Potato

Fig. 3 shows the measured dynamics of changes in T_2 relaxation times in the inner and outer medulla of the potato exposed to the PEF treatment. Fig. 3A, C show a baseline T_2 – weighted image of a potato tuber before it was exposed to PEF treatment with a marked area where potato was exposed to an electric field greater than 250 V/cm. This electric field value was chosen as a threshold based on previous report in which a consistent decrease in the T_2 value was only achieved in the potato tuber exposed to electric fields greater than 250 V/cm (Genovese et al., 2021). Each of the evaluated regions of interest were divided into the area exposed to electric fields greater than 250 V/cm ($R1_{in,}$ $R1_{out}$ in Fig. 3, where subscripts *in* and *out* stand for inner and outer medulla, respectively) and the area exposed to electric fields lower than 250 V/cm ($R2_{in,}$ $R2_{out}$ in Fig. 3). In addition, Fig. 3B shows the dynamics of T_2 changes in the inner medulla or water pith, while the Fig. 3D shows the dynamics in the outer medulla of the potato (note different ranges of T_2 in Fig. 3B and D). At time 0, i.e. before application of PEF, different initial T_2 value within same structure can be observed. That is in agreement with inhomogeneous distribution of T_2 relaxation times of tissue structures also observed in Fig. 1B (in case of potato structures, inner medulla has baseline T_2 times between 200 and 350 ms, while outer medulla between 120 and 180 ms).

In Fig. 3B, it can be observed that the inner medulla of the potato is the region most affected by the PEF treatment. The $R1_{in}$ shows a continuous and significant decrease in T_2 values after the application of the high-voltage pulses during the 6 h follow-up. In contrast, the part of the medulla exposed to electric fields lower than the threshold (i.e. 250 V/cm) shows a statistically significant increase in T_2 relaxation times, starting 2 h after the PEF treatment ($R2_{in}$ in Fig. 3B). This increase in T_2 values indicates that, after PEF treatment, the water starts to redistribute within the vascular system and starts diffusing out from the electroporated area (i.e. area exposed to high electric field) towards the edges of the sample (i.e. area of low electric field).

The outer medulla of the potato tuber exhibits smaller but still significant decrease in the absolute and relative value of T_2 than the inner medulla. A slow decrease in T_2 values is only observed in the region exposed to electric field strengths above the threshold ($R1_{out}$ in Fig. 3D), while no statistically significant changes in T_2 values are observed in the regions below the electroporation threshold ($R2_{out}$ in Fig. 3D). The results of statistical analysis obtained with ANOVA are shown in Table S-1.

In potato tuber, the change in T_2 following PEF treatment is strongly structure-dependent, with the inner medulla being the tissue region where most of the water is drained out due to electroporation of the cell membranes (i.e. greater decrease in T_2). In the outer medulla region, high values of electric field were reached (i.e. 450–500 V/cm, $R1_{out}$ in Fig. 3C), but the decrease in T_2 relaxation times is much smaller. Therefore, the inhomogeneities of the cell structure in the potato tissue affect the consequences of electroporation in terms of water mobility and water interactions with the surrounding macromolecules.

3.4. Carrot

Fig. 4 shows the measured dynamics of changes in T_2 relaxation times in the tissue structures of the carrot exposed to the PEF treatment. T_2-maps of carrot allowed differentiation of various tissue structures based on different transverse relaxation times of their cells containing said structures. The cortex tissue was characterised by much shorter relaxation times (i.e. in the range of 50–65 ms) than xylem and cambium (Fig. 4A, B). The cambium is easily recognised as the bright ring surrounding the central core cylinder with the xylem (Fig. 4E, F). The xylem tissue inside the ring of cambium was characterised by longer T_2 relaxation times (i.e. in the range of 250–300 ms, Fig. 4C, 4D). Interestingly, as in potato tuber, T_2 relaxation times changes of carrot structures were visible in areas exposed to an electric field greater than 250 V/cm. Therefore, each of the evaluated regions of interest were divided into the area exposed to electric fields greater than 250 V/cm ($R1_{cx,xy,cb,vr}$ in Fig. 4, where subscripts stand for the different tissue structures of carrot) and the area exposed to electric fields lower than 250 V/cm ($R2_{cx,xy,cb,vr}$ in Fig. 4). In the parenchyma cortex exposed to electric fields above the threshold, the T_2 relaxation time shows an abrupt and significant increase after the application of PEF treatment (i.e. after 18 min), indicating that water protons undergo an increase in mobility (Fig. 4B). As a confirmation, no statistically significant change in T_2 relaxation times is observed when the cortex was exposed to electric fields of less than 250 V/cm (i.e. $R2_{cx}$ in Fig. 4B). The same trend is observed in the cambium ring, displayed in Fig. 4F, where significant increase in T_2 times is observed 18 min after the application of electroporation pulses with an electric field greater than 250 V/cm. On the other hand, the xylem tissue (Fig. 4D), characterised by a higher amount of free water (hence longer T_2 time) and by cells of almost uniform shape and size, shows a significant decrease in T_2 times after the application of PEF treatment in the areas exposed to higher electric fields ($E > 250$ V/cm, $R1_{xy}$ in Fig. 4D). Interestingly, T_2 values in the area of xylem exposed to lower electric field strengths significantly increase immediately after the PEF treatment $R2_{xy}$ (Fig. 4D). Thus, we can speculate that the central core cylinder of the carrot (i.e. the vascular system of the taproot) might have a lower electroporation threshold than the other tissue structures. The results of statistical analysis obtained with ANOVA are shown in Table S-1. Changes of T_2 values in the vascular rays of the carrot due to the PEF treatment (Fig. 4G, 4H) are addressed in Section 3.6.

The dynamics of changes in relaxation times after the application of PEF treatment showed that different tissue structures of the carrot exposed to the electric field greater than 250 V/cm resulted in a homogenisation of T_2 values around 100–150 ms. This effect is clearly visible in the T_2-weighted image scanned 6 h after the PEF treatment (Fig. 5B). While the T_2 values in the image scanned before the PEF treatment (Fig. 5A) have much broader distribution with the T_2 values in the range between 90 and 350 ms, this distribution becomes narrower 6 h after the application of the electroporation pulses (Fig. 5B) where the xylem and the vascular rays in the marked area can hardly be distinguished from the parenchyma tissue of the cortex and cambium. T_2 homogenisation effect is also evident in a narrower distribution of T_2 values in the areas exposed to PEF treatment (Fig. 5C).

3.5. Spatial distribution of electroporation in tissue structures

It has been reported that changes in T_2 relaxation times can be used to quantify the effect of electroporation in plant tissues (Dellarosa et al., 2016; Kranjc et al., 2016). Electroporation pulses lead to structural changes, such as damage to cell membranes, and thus alter the interior of the cells as well as the extracellular environment, which in turn affect the proton relaxation times. As described by Hills & Duce (1990), in biological systems the diffusion of water between cell compartments and also the proton chemical exchange between water and other solutes are often the processes that predominantly influence the proton relaxation times. Furthermore, the proton signal of plant tissues is characterised by multiexponential decays, thus reflecting the information of different cell compartments, with a different water content and water physical properties (Mariette et al., 2012; Van As & Van Duynhoven, 2013). The primary effect of electroporation is associated with the cell membrane disruption and loss of compartmentalisation, leading to a redistribution

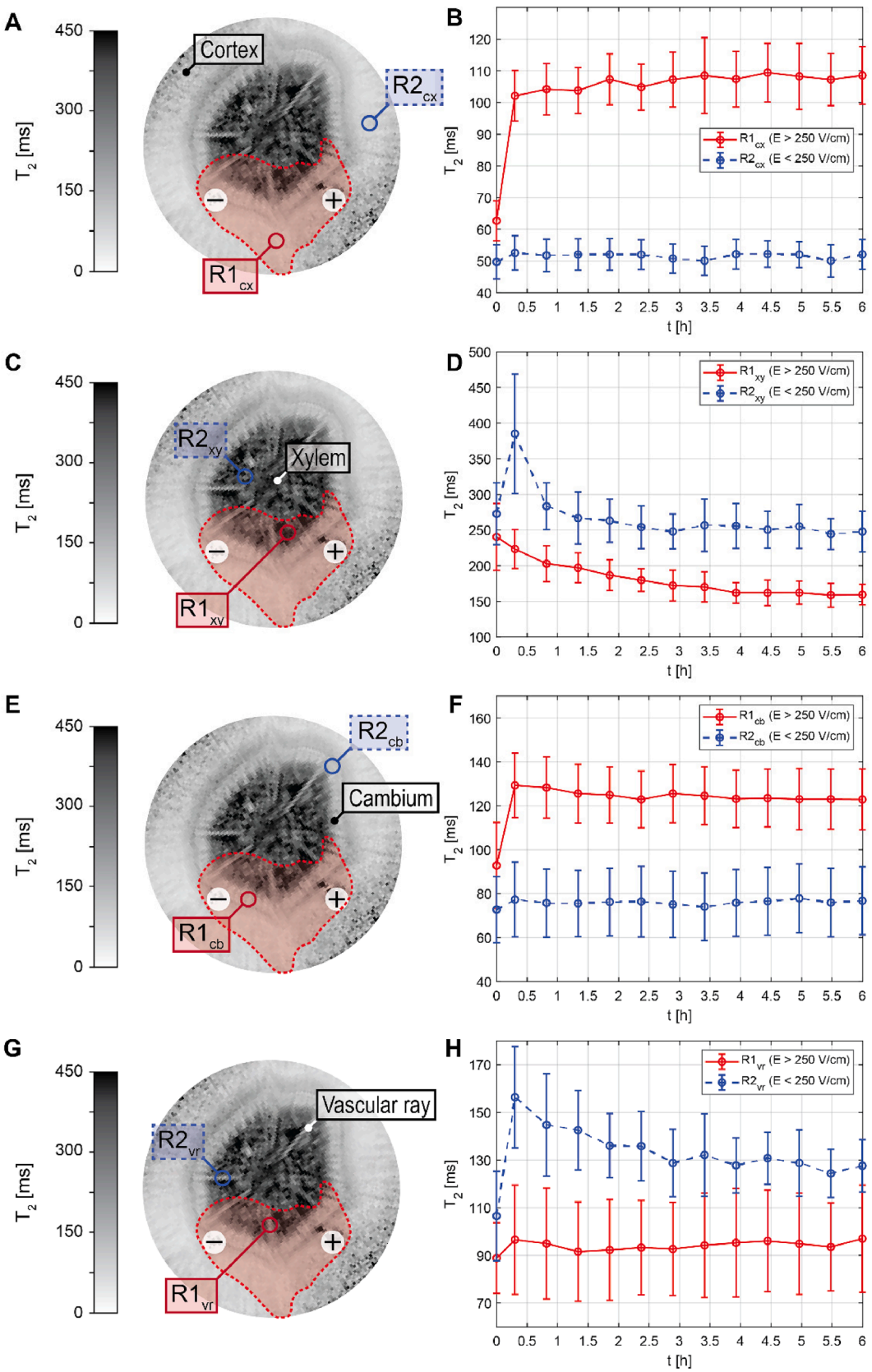

Fig. 4. Evaluation of T_2 values in the cortex, xylem, cambium, and vascular rays of the carrot exposed to PEF. **A, C, E, G**: An area of the carrot that was exposed to an electric field greater than 250 V/cm is shaded in red. T_2 values were evaluated in two Regions of interest in the cortex (R1-2$_{cx}$), in the xylem (R1-2$_{xy}$), in the cambium (R1-2$_{cb}$), and in the vascular rays (R1-2$_{vr}$). R1$_{cx,xy,cb,vr}$ and R2$_{cx,xy,cb,vr}$ were in the regions exposed to an electric field greater and less than 250 V/cm, respectively. The locations of the electrodes are marked with + and -. **B, D, F, H**: Time course of T_2 values within R1$_{cx,xy,cb,vr}$ and R2$_{cx,xy,cb,vr}$. Each time point represents a mean of T_2 ± standard deviation from the region of interest. Time point $t = 0$ shows T_2 values before the application of PEF. Note different ranges of T_2 in B, D, F, H.

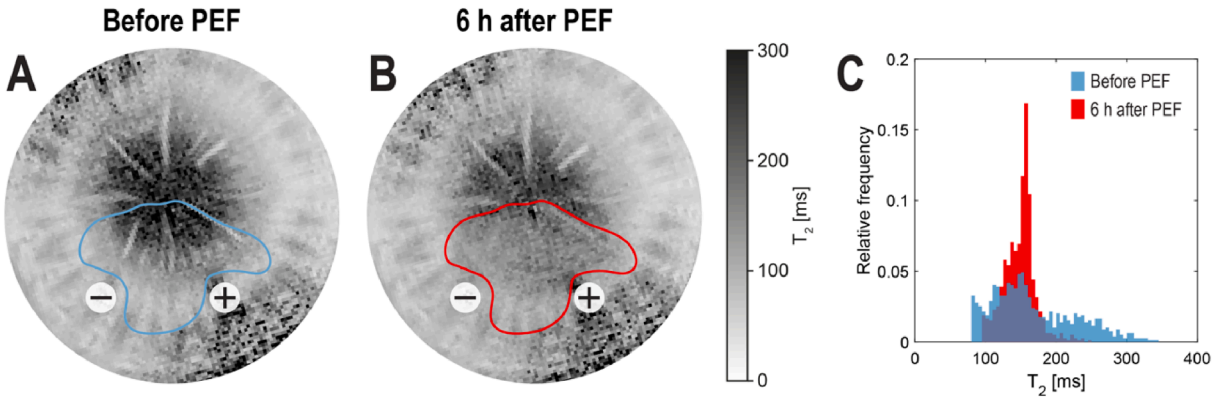

Fig. 5. Comparison of T_2 values before and after the application of PEF. **A**: T_2 - weighted image of carrot before the application of PEF. **B**: T_2 - weighted image of carrot after 6 h of application of PEF. **C**: Distribution of T_2 values within the blue and red marked areas. The blue and red marked areas include all different tissue structures of the carrot exposed to the electric field greater than 250 V/cm.

of water between different compartments and tissue structures and also to a significant change in water-solutes interactions (Lebovka et al., 2002). In our study, these changes, triggered by PEF treatment, were spatially visualised by T_2 mapping. Above the electroporation threshold, in the apple, potato, and carrot, the increased permeability of cell membranes, tonoplast and plasma membrane, likely contributed to a redistribution of water and increased diffusion from sites of low resistance to water permeation (i.e. vascular bundles) to high ones (i.e. cortex). The dynamics of changes for all plant tissues can be seen in videos within Supplementary material. The shortening of T_2 relaxation times could be due to the loss of magnetisation of protons, which results from the faster exchange of water as it crosses the vacuolar membrane towards the cytoplasm and extracellular space. Protons lose their magnetisation in the cytoplasm and cell wall (Donker et al., 1996). This phenomenon is clearly visible in apple tissue after the PEF treatment (i.e. 18 min after pulsation) and leads to a 17 % reduction in T_2 relaxation times in the tissue areas where electric fields between 700 and 1700 V/cm were reached (Fig. 2). As noted before, PEF treatment of apples led to a collapse of cell structure (vacuole and cytoplasmatic space), which in turn led to a redistribution of cell contents and a different interaction between water and macromolecules, possibly contributing to a systematic reduction in T_2 (Dellarosa et al., 2016, 2018). Furthermore, it is important to highlight that apple tissue is characterised by high porosity (higher than potato and carrot tissues) with air-filled intercellular spaces (Madiouli et al., 2012). Since gas and water have different magnetic susceptibilities, internal magnetic gradients occur at the air-water interface around the intercellular air gaps (Duce et al., 1992). The diffusion of water molecules through these internal magnetic gradients is responsible for the loss of signal intensity (i.e. shorter T_2 relaxation time).

In tissues with more complex structures, such as potato and carrot, the difference in signal intensity between the vascular system and the surrounding parenchyma provided information about the inhomogeneous effect of PEF treatment. The higher T_2 values of the vascular systems (inner medulla in potato and xylem in carrot) indicate the presence of bulk water. In these areas (specifically at $E > 250$ V/cm) the observed higher rate of proton magnetisation loss (i.e. decrease in T_2) may indicate an increase in the rate of water exchange between the cytoplasm and intercellular spaces after the application of PEF pulses and during the subsequent 6 h.

In carrot, parenchyma cortex is largely composed of parenchyma cells storing sugars (mainly glucose, fructose, and sucrose), and it is possible that here the water molecules and sugars interact more intensely, which can explain the shorter initial T_2 of carrot cortex (between 45 and 70 ms) compared to apple and potato parenchyma (between 105–130 ms and 120–170 ms, respectively). The application of the PEF treatment triggered the possible release of sugars, as already shown before (Aguiló-Aguayo et al., 2014), leading to variations in the water-sugar interactions and the proton exchange, and therefore contributing significantly, along with the increase of localised water content, to the observed increase in T_2 after PEF treatment in the parenchyma cortex (Fig. 4B). Similar increase of T_2 after PEF treatment can also be observed in cambium (Fig. 4F).

3.6. Limitations of the study

The experimental setup for MR imaging used in our study provided images with a pixel size of 469 × 469 μm for the electric field distribution and 234 × 234 μm for the T_2 maps. Although the achieved spatial resolution of MRI allowed the observation of most structures used in our study, the pixel size is still too large for observation of smaller structures such as the rays in the xylem of a carrot, as shown by the high standard deviations of T_2 relaxation time in Fig. 4H. Another technical limitation is related to MREIT algorithm used in this study; it reconstructs plant tissue conductivity as isotropic, even though plants such as carrot exhibit anisotropic behaviour (Pacheco-Aguirre et al., 2014).

4. Conclusion

In this paper, we analyse the change in T_2 relaxation times due to PEF treatment to investigate the non-uniform effect of electroporation due to the structural heterogeneity of plant tissues. We believe our study has successfully and conclusively demonstrated feasibility and considerable potential for the use of T_2 mapping MRI technique in analysis of plant tissue structures, especially when studying the plant tissue response to electroporation/PEF treatment. This imaging method facilitates multiple possible novel approaches (stand-alone and combined) to analysis of the PEF-treated tissue, since it allows for a contactless and a non-invasive imaging of water mobility and water-solute interactions which are of major importance in all applications of PEF in food technology where enhancing mass transport is the primary objective of the electrical (pre)treatment.

Being able to analyse the water distribution and redistribution within the electroporated tissue is of importance not only for determining the treatment intensity and the fitness for purpose of a specific treatment protocol in a particular food matrix, but also for basic studies of material properties and their modification as a consequence of processing by using emerging technologies. In this case, the technique offers new means of visualising and quantitatively studying phenomena induced in turgid plant tissues by means of electroporation and correlating these observations with other, previously established methods of experimental study, such as texture analysis and electrical impedance spectroscopy.

In previous works in the field of PEF applications for food

technology, electrical impedance and/or textural response of tissue to PEF treatment have been extensively studied and have been proposed as methods of characterising the degree to which electrical treatment affects (damages) the raw plant material (Boussetta et al., 2009; Genovese et al., 2021; Lebovka et al., 2002; Mahnič-Kalamiza et al., 2015). Some of these observations made in the mentioned studies call for intricate explanations involving effects of PEF on water redistribution in tissue, and the approach demonstrated in this paper can be thought of as a complimentary method of significant potential and explanatory power that can be used to corroborate hypotheses made in the past as to how electroporation affects plant tissue.

CRediT authorship contribution statement

Jessica Genovese: Conceptualization, Methodology, Investigation, Data curation, Writing – original draft, Writing – review & editing. **Marko Stručić:** Investigation, Methodology, Software, Writing – original draft. **Igor Serša:** Methodology, Software, Resources, Writing – original draft. **Vitalij Novickij:** Methodology, Writing – original draft. **Pietro Rocculi:** Writing – original draft, Supervision, Funding acquisition. **Damijan Miklavčič:** Writing – original draft, Resources, Supervision, Funding acquisition. **Samo Mahnič-Kalamiza:** Writing – original draft, Supervision. **Matej Kranjc:** Investigation, Methodology, Data curation, Visualization, Software, Writing – original draft, Writing – review & editing, Supervision, Funding acquisition.

Declaration of Competing Interest

The authors declare that they have no known competing financial interests or personal relationships that could have appeared to influence the work reported in this paper.

Data availability

Data will be made available on request.

Acknowledgments

The author JG would like to acknowledge the financial support provided by *Marco Polo Mobility Programme* funded by Department of Agricultural and Food Sciences of University of Bologna to conduct the presented study at University of Ljubljana. The authors DM, SMK, and MK would like to acknowledge the financial support through research programs and projects granted by the Slovenian Research Agency (ARRS), namely the research program P2-0249, the funding for Junior Researcher to MS, the postdoctoral project Z7-1886 (awarded to SMK), and research project J2-1733 (awarded to MK). This study was conducted within Infrastructure Program: Network of research infrastructure centres at the University of Ljubljana (MRIC UL IP-0510).

Appendix A. Supplementary data

Supplementary data to this article can be found online at https://doi.org/10.1016/j.foodchem.2022.134892.

References

Aguiló-Aguayo, I., Downey, G., Keenan, D. F., Lyng, J. G., Brunton, N., & Rai, D. K. (2014). Observations on the water distribution and extractable sugar content in carrot slices after pulsed electric field treatment. *Food Research International, 64*, 18–24. https://doi.org/10.1016/J.FOODRES.2014.06.011

Boussetta, N., Lebovka, N., Vorobiev, E., Adenier, H., Bedel-Cloutour, C., & Lanoisellé, J. L. (2009). Electrically assisted extraction of soluble matter from chardonnay grape skins for polyphenol recovery. *Journal of Agricultural and Food Chemistry*. https://doi.org/10.1021/jf802579x

Campana, L. G., Dughiero, F., Forzan, M., Rossi, C. R., & Sieni, E. (2016). A prototype of a flexible grid electrode to treat widespread superficial tumors by means of Electrochemotherapy. *Radiology and Oncology, 50*(1), 49–57. https://doi.org/10.1515/RAON-2016-0013

Canelli, G., Kuster, I., Jaquenod, L., Buchmann, L., Murciano Martínez, P., Rohfritsch, Z., … Mathys, A. (2022). Pulsed electric field treatment enhances lipid bioaccessibility while preserving oxidative stability in Chlorella vulgaris. *Innovative Food Science & Emerging Technologies, 75*, Article 102897. https://doi.org/10.1016/J.IFSET.2021.102897

Carr, H. Y., & Purcell, E. M. (1954). Effects of diffusion on free precession in nuclear magnetic resonance experiments. *Physical Review, 94*(3), 630–638. https://doi.org/10.1103/PhysRev.94.630

Collewet, G., Musse, M., El Hajj, C., & Moussaoui, S. (2022). Multi-exponential MRI T2 maps: A tool to classify and characterize fruit tissues. *Magnetic Resonance Imaging, 87*, 119–132. https://doi.org/10.1016/j.mri.2021.11.018

Dellarosa, N., Laghi, L., Ragni, L., Dalla Rosa, M., Galante, A., Ranieri, B., … Alecci, M. (2018). Pulsed electric fields processing of apple tissue: Spatial distribution of electroporation by means of magnetic resonance imaging and computer vision system. *Innovative Food Science and Emerging Technologies*. https://doi.org/10.1016/j.ifset.2018.02.010

Dellarosa, N., Ragni, L., Laghi, L., Tylewicz, U., Rocculi, P., & Dalla Rosa, M. (2016). Time domain nuclear magnetic resonance to monitor mass transfer mechanisms in apple tissue promoted by osmotic dehydration combined with pulsed electric fields. *Innovative Food Science & Emerging Technologies, 37*, 345–351. https://doi.org/10.1016/j.ifset.2016.01.009

Donker, H. C. W., Van As, H. T., Edzes, H. T., & Jans, A. W. H. (1996). NMR imaging of white button mushroom (Agaricus bisporis) at various magnetic fields. *Magnetic Resonance Imaging, 14*(10), 1205–1215. https://doi.org/10.1016/S0730-725X(96)00143-9

Duce, S. L., Carpenter, T. A., Hall, L. D., & Hills, B. P. (1992). An investigation of the origins of contrast in NMR spin echo images of plant tissue. *Magnetic Resonance Imaging, 10*(2). https://doi.org/10.1016/0730-725X(92)90488-L

Esau, K. (1940). Developmental anatomy of the fleshy storage organ of Daucus carota. *Hilgardia, 13*(5), 175–226. https://doi.org/10.3733/hilg.v13n05p175

Gagneten, M., Leiva, G., Salvatori, D., Schebor, C., & Olaiz, N. (2019). Optimization of pulsed electric field treatment for the extraction of bioactive compounds from blackcurrant. *Food and Bioprocess Technology, 12*(7), 1102–1109. https://doi.org/10.1007/s11947-019-02283-1

Genovese, J., Kranjc, M., Serša, I., Petracci, M., Rocculi, P., Miklavčič, D., & Mahnič-Kalamiza, S. (2021). PEF-treated plant and animal tissues: Insights by approaching with different electroporation assessment methods. *Innovative Food Science and Emerging Technologies, 74*(November). https://doi.org/10.1016/j.ifset.2021.102872

Genovese, J., Tappi, S., Luo, W., Tylewicz, U., Marzocchi, S., Marziali, S., … Rocculi, P. (2019). Important factors to consider for acrylamide mitigation in potato crisps using pulsed electric fields. *Innovative Food Science & Emerging Technologies, 55*. https://doi.org/10.1016/j.ifset.2019.05.008

Hills, B. (1995). Food processing: An MRI perspective. *In Trends in Food Science and Technology*. https://doi.org/10.1016/S0924-2244(00)88993-1

Hills, B. P., & Duce, S. L. (1990). The influence of chemical and diffusive exchange on water proton transverse relaxation in plant tissues. *Magnetic Resonance Imaging, 8*(3), 321–331. https://doi.org/10.1016/0730-725X(90)90106-C

Hjouj, M., & Rubinsky, B. (2010). Magnetic resonance imaging characteristics of nonthermal irreversible electroporation in vegetable tissue. *The Journal of Membrane Biology, 236*(1), 137–146. https://doi.org/10.1007/s00232-010-9281-2

Joy, M., Scott, G., & Henkelman, M. (1989). In vivo detection of applied electric currents by magnetic resonance imaging. *Magnetic Resonance Imaging*, 89–94. https://doi.org/10.1016/0730-725X(89)90328-7

Kamal, T., Cheng, S., Khan, I. A., Nawab, K., Zhang, T., Song, Y., … Tan, M. (2019). Potential uses of LF-NMR and MRI in the study of water dynamics and quality measurement of fruits and vegetables. *Journal of Food Processing and Preservation, 43*(11). https://doi.org/10.1111/jfpp.14202

Khang, H. S., Lee, B. I., Oh, S. H., Woo, E. J., Lee, S. Y., Cho, M. H., … Seo, J. K. (2002). J-substitution algorithm in magnetic resonance electrical impedance tomography (MREIT): Phantom experiments for static resistivity images. *IEEE Transactions on Medical Imaging, 21*(6). https://doi.org/10.1109/TMI.2002.800604

Kotnik, T., Kramar, P., Pucihar, G., Miklavčič, D., & Tarek, M. (2012). Cell membrane electroporation - Part 1: The phenomenon. *IEEE Electrical Insulation Magazine, 28*(5), 14–23. https://doi.org/10.1109/MEI.2012.6268438

Kotnik, T., Rems, L., Tarek, M., & Miklavcic, D. (2019). Membrane Electroporation and Electropermeabilization: Mechanisms and Models. In *Annual Review of Biophysics* (Vol. 48). 10.1146/annurev-biophys-052118-115451.

Kranjc, M., Bajd, F., Sersa, I., Woo, E. J., & Miklavcic, D. (2012). Ex vivo and in silico feasibility study of monitoring electric field distribution in tissue during electroporation based treatments. *PLoS ONE, 7*(9), e45737.

Kranjc, M., Bajd, F., Sersa, I., & Miklavcic, D. (2011). Magnetic resonance electrical impedance tomography for monitoring electric field distribution during tissue electroporation. *IEEE Transactions on Medical Imaging, 30*(10), 1771–1778. https://doi.org/10.1109/TMI.2011.2147328

Kranjc, M., Bajd, F., Serša, I., de Boevere, M., & Miklavčič, D. (2016). Electric field distribution in relation to cell membrane electroporation in potato tuber tissue studied by magnetic resonance techniques. *Innovative Food Science & Emerging Technologies, 37*, 384–390. https://doi.org/10.1016/j.ifset.2016.03.002

Lebovka, N. I., Bazhal, M. I., & Vorobiev, E. (2002). Estimation of characteristic damage time of food materials in pulsed-electric fields. *Journal of Food Engineering*. https://doi.org/10.1016/S0260-8774(01)00220-5

Madiouli, J., Sghaier, J., Lecomte, D., & Sammouda, H. (2012). Determination of porosity change from shrinkage curves during drying of food material. *Food and Bioproducts Processing, 90*(1), 43–51. https://doi.org/10.1016/J.FBP.2010.12.002

Mahnič-Kalamiza, S., & Miklavčič, D. (2022). The phenomenon of electroporation. In *Pulsed Electric Fields Technology for the Food Industry* (pp. 107–141). Springer. https://doi.org/10.1007/978-3-030-70586-2_3.

Mahnič-Kalamiza, S., Miklavčič, D., & Vorobiev, E. (2014). Dual-porosity model of solute diffusion in biological tissue modified by electroporation. *Biochimica et Biophysica Acta (BBA) - Biomembranes, 1838*(7), 1950–1966. https://doi.org/10.1016/J.BBAMEM.2014.03.004

Mahnič-Kalamiza, S., Miklavčič, D., & Vorobiev, E. (2015). Dual-porosity model of mass transport in electroporated biological tissue: Simulations and experimental work for model validation. *Innovative Food Science and Emerging Technologies*. https://doi.org/10.1016/j.ifset.2014.09.011

Mahnič-Kalamiza, S., Vorobiev, E., & Miklavčič, D. (2014). Electroporation in food processing and biorefinery. *Journal of Membrane Biology, 247*(12), 1279–1304. https://doi.org/10.1007/s00232-014-9737-x

Mariette, F., Collewet, G., Davenel, A., Lucas, T., & Musse, M. (2012). Quantitative MRI in food science & food engineering. In *Encyclopedia of Magnetic Resonance* (Vol. 1, pp. 205–214). John Wiley & Sons Ltd. https://doi.org/10.1002/9780470034590.emrstm1272.

Menegazzo, I., Mammi, S., Sgarbossa, P., Bartolozzi, A., Mozzon, M., Bertani, R., … Sieni, E. (2020). Time Domain Nuclear Magnetic Resonance (TD-NMR) to evaluate the effect of potato cell membrane electroporation. *Innovative Food Science & Emerging Technologies, 65*, Article 102456. https://doi.org/10.1016/J.IFSET.2020.102456

Novickij, V., Grainys, A., Butkus, P., Tolvaišienė, S., Švedienė, J., Paškevičius, A., & Novickij, J. (2016). High-frequency submicrosecond electroporator. *Biotechnology and Biotechnological Equipment*. https://doi.org/10.1080/13102818.2016.1150792

Pacheco-Aguirre, F. M., Ladrón-González, A., Ruiz-Espinosa, H., García-Alvarado, M. A., & Ruiz-López, I. I. (2014). A method to estimate anisotropic diffusion coefficients for cylindrical solids: Application to the drying of carrot. *Journal of Food Engineering, 125*(1), 24–33. https://doi.org/10.1016/J.JFOODENG.2013.10.015

Patel, K. K., Khan, M. A., & Kar, A. (2015). Recent developments in applications of MRI techniques for foods and agricultural produce—An overview. *Journal of Food Science and Technology, 52*(1), 1–26. https://doi.org/10.1007/s13197-012-0917-3

Praporscic, I., Lebovka, N., Vorobiev, E., & Mietton-Peuchot, M. (2007). Pulsed electric field enhanced expression and juice quality of white grapes. *Separation and Purification Technology, 52*(3), 520–526. https://doi.org/10.1016/J.SEPPUR.2006.06.007

R. M. Reeve, E. H. A. M. L. W. (1969). Anatomy and compositional variation within potatoes: Developmental histology of the tuber. *American Potato Journal, 46*(361–373).

Schouten, M. A., Genovese, J., Tappi, S., Di Francesco, A., Baraldi, E., Cortese, M., … Romani, S. (2020). Effect of innovative pre-treatments on the mitigation of acrylamide formation in potato chips. *Innovative Food Science & Emerging Technologies, 64*, Article 102397. https://doi.org/10.1016/J.IFSET.2020.102397

Seo, J. K., & Woo, E. J. (2014). Electrical tissue property imaging at low frequency using MREIT. *IEEE Transactions on Biomedical Engineering, 61*(5). https://doi.org/10.1109/TBME.2014.2298859

Serša, I. (2008). Auxiliary phase encoding in multi spin-echo sequences: Application to rapid current density imaging. *Journal of Magnetic Resonance*. https://doi.org/10.1016/j.jmr.2007.10.009

Serša, I., Jarh, O., & Demsar, F. (1994). Magnetic resonance microscopy of electric currents. *Journal of Magnetic Resonance, Series A, 111*(1), 93–99. https://doi.org/10.1006/JMRA.1994.1230

Tylewicz, U., Mannozzi, C., Castagnini, J. M., Genovese, J., Romani, S., Rocculi, P., & Rosa, M. D. (2022). Application of PEF- and OD-assisted drying for kiwifruit waste valorisation. *Innovative Food Science & Emerging Technologies, 77*, Article 102952. https://doi.org/10.1016/J.IFSET.2022.102952

Van As, H., & Van Duynhoven, J. (2013). MRI of plants and foods. *Journal of Magnetic Resonance*. https://doi.org/10.1016/j.jmr.2012.12.019

Wiktor, A., Nowacka, M., Dadan, M., Rybak, K., Lojkowski, W., Chudoba, T., & Witrowa-Rajchert, D. (2016). The effect of pulsed electric field on drying kinetics, color, and microstructure of carrot. *Drying Technology, 34*(11), 1286–1296. https://doi.org/10.1080/07373937.2015.1105813